Behavior of Extended Single-Plate Shear Connections Subjected to Combined Shear and Compression Forces Using Finite Element Analysis

SUNIL SAPKOTA, GIAN ANDREA RASSATI, JAMES A. SWANSON, and BO DOWSWELL

ABSTRACT

Extended single-plate shear connections can be subjected to compression loads in addition to shear loads during extreme events like wind and earthquakes. However, the existing interaction equations found in the AISC *Steel Construction Manual* (2023), in literature, and in design examples—which are being used in design for combined loading cases—have not been formally validated for use by experimental testing or finite element analysis. This research aims to study the behavior of these connections when subjected to combined loading of shear and compression force by performing a nonlinear finite element analysis in ABAQUS (2022). The variables considered in the study are column web stiffness, connection configurations, and different bracing conditions of the beam. The results from these analyses were compared to the available interaction equations in the AISC *Manual* and in literature to assess their applicability under different conditions. Shear-compression interaction plots were generated from the results that show the shear strength decreases with an increase in compression force in the connection. The effect of the compression force on the shear strength depends on the column web's rigidity and the bracing condition of the beam.

Keywords: extended shear tabs, finite element analysis (FEA), combined loading, compression, shear, interaction equations.

INTRODUCTION

Single-plate shear connections offer many advantages over other connection configurations: They are cost effective, are easy to fabricate, and provide rapid erection capabilities. However, when the supported beam needs to be connected to the web of the girder or the web of the supporting column, the ends of the beam may need to be coped as shown in Figure 1(a). Coping makes the fabrication process difficult and expensive, which takes away the advantages that these connections offer.

Coping can be avoided by extending the plate beyond the flange of the supporting column or girder. This causes the *a* distance [the distance between weld line and bolt line as shown in Figure 1(a)] to be longer than the limit set for conventional shear tabs; such configuration of the shear tab is known as extended single-plate shear connection, or extended shear tab, and is shown in Figure 1(b). The major benefit of these connections is that the fabrication process is simple, and erection work is faster as coping of the beam is avoided. Owing to the larger length compared to conventional shear tabs, they have higher eccentricity, resulting in a higher moment in the connection. This makes the behavior of extended shear tabs different than the conventional configurations, resulting in additional failure modes and limit states that need to be considered.

Two types of conceptual support conditions may exist for these connections—rigid and flexible. When a shear tab is attached to the column flange or connected to both sides of the girder or column web, the support is considered rigid (Muir and Hewitt, 2009). The extended shear tabs that are connected on only one side of the column web or girder web are considered to have a flexible support condition. The support condition affects the behavior of these connections as it influences the point of inflection of the in-plane moment, which ultimately affects the moment to which the bolt group is subjected. In some extended shear tabs, stabilizer plates are provided to improve the stability of the connection as shown in Figure 2. These configurations are called stiffened extended shear tabs, and the ones without any stabilizer plates are called unstiffened extended shear tabs.

The actual moment developed in the plate and bolt group is difficult to estimate because there is an uncertainty in the actual rigidity of the supports, and it is difficult to find the exact stiffness of the connection. Research done in the

Sunil Sapkota, Graduate Structural Engineer, JPS Consulting Engineers LLC, Indianapolis, Ind. Email: sunil@jpsconsultingengineers.com

Gian Andrea Rassati, PhD, Associate Professor, Department of Civil and Architectural Engineering and Construction Management, University of Cincinnati, Cincinnati, Ohio. Email: rassatga@ucmail.uc.edu (corresponding)

James A. Swanson, PhD, Associate Professor, Department of Civil and Architectural Engineering and Construction Management, University of Cincinnati, Cincinnati, Ohio. Email: swansojs@ucmail.uc.edu

Bo Dowswell, PhD, PE, Principal, ARC International, LLC, Birmingham, Ala. Email: bo@arcstructural.com

Paper No. 2024-02

past has focused on the study of failure modes, shear load eccentricity, support rotation, and stability of the extended shear tabs. Most of the studies were focused on the case of gravity-induced shear load alone. However, in certain cases connections are expected to carry axial load as well as shear load, and their combined presence will affect the behavior of the connection. One of the most common sources of axial load in connections is lateral load (wind or earthquake load). Axial load is developed in the connection when a supported member is a part of the lateral load-resisting path. Similarly, for gable-shaped buildings, axial forces can be developed in the connection. Furthermore, an extreme load

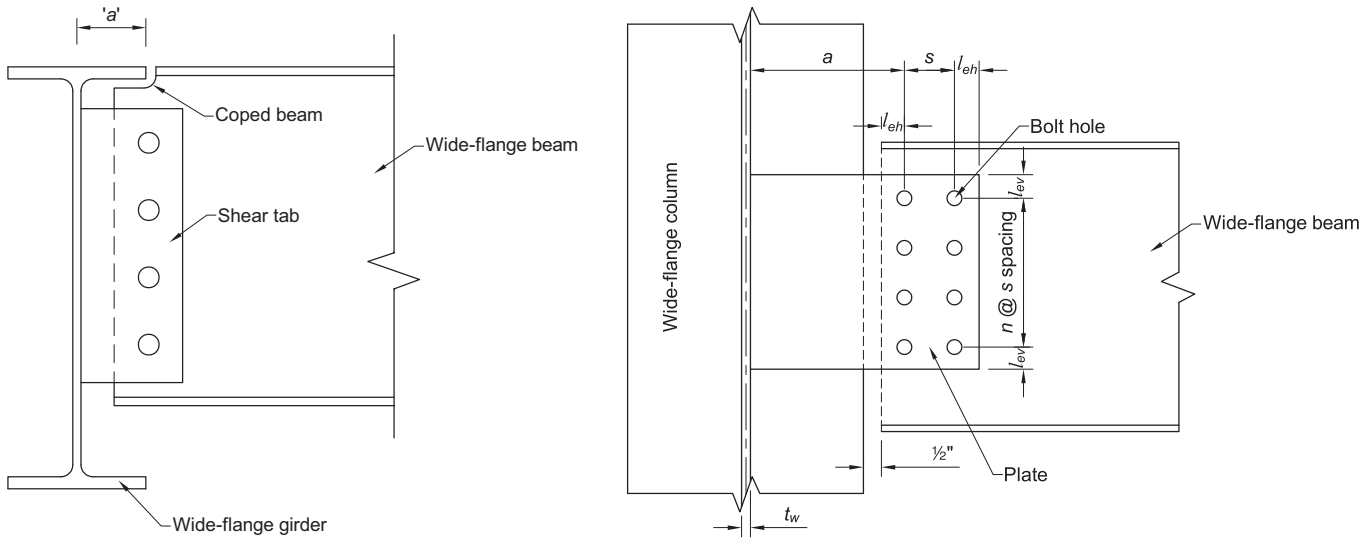

(a) Coped beam-to-girder connection (Asl et al., 2019) *(b) Unstiffened extended single-plate shear connection*

Fig. 1. Single-plate shear connections.

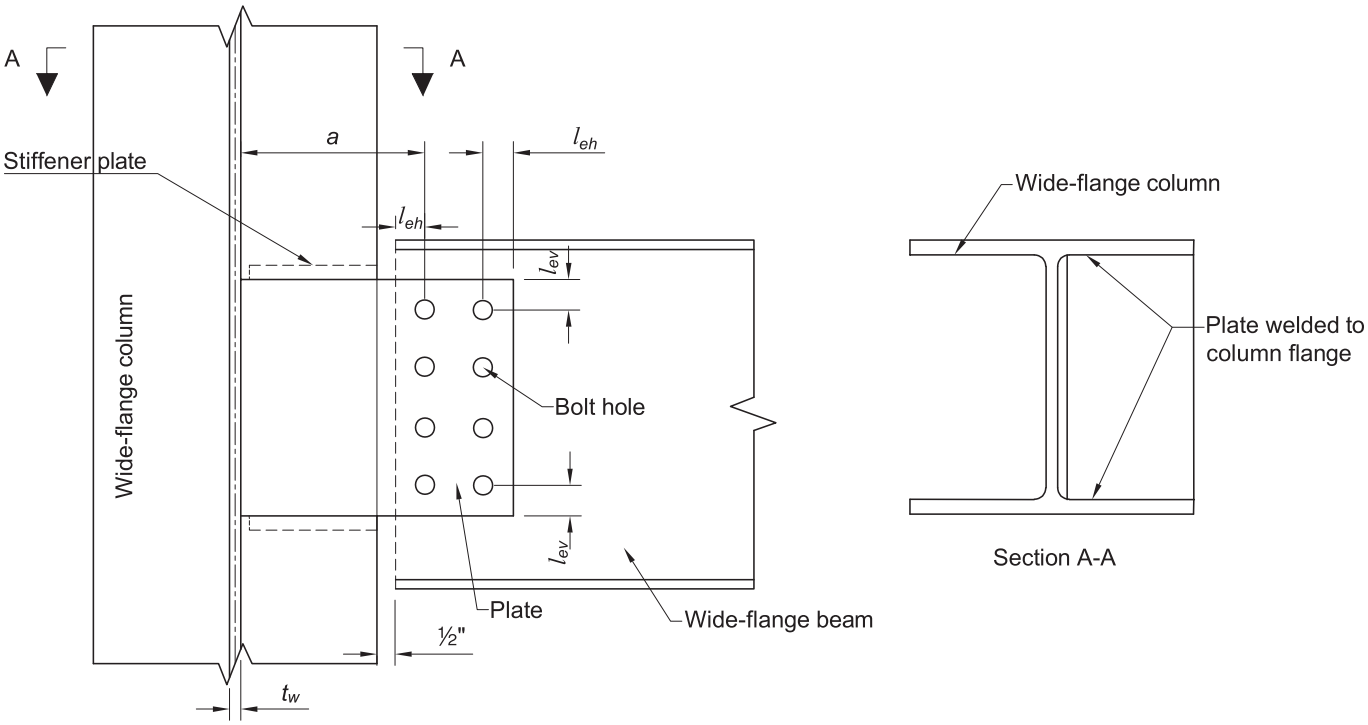

Fig. 2. Stiffened extended shear tab connected to column web.

event such as a blast or a fire may lead to the development of axial forces that will need to be transferred through the connection, due, for example, to the emergence of catenary action in the beam or to the loss of a column. There are very few studies that examine the behavior of these connections under combined shear and axial forces. This research focuses on the study of the behavior of unstiffened extended shear tabs connected to the web of a column under a combined loading of shear and axial compression forces.

BACKGROUND

Past Research on Combined Loading

Mirzaei (2014) conducted four full-scale experimental tests of conventional shear tabs for combined loading of shear and axial force in order to improve the design procedure for shear tabs in Canadian specifications. The experimental testing was followed by a parametric study in ABAQUS (2022), which showed that adding a small compression load increased the shear strength, but beyond a certain range, the strength decreased. Conversely, the addition of tensile force decreased the shear strength. This behavior was attributed to the compression load delaying the weld tearing, while the addition of tensile load put higher demands on the weld, resulting in weld failure.

Thomas (2014) performed full-scale testing on 23 extended shear tabs, 12 of which were subjected to combined loading of shear and axial forces. The major parameters studied were tab depth, tab thickness, and presence of stiffeners. The support condition was flexible because the plates were welded single sided to a web of a column stub. The failure mode for tensile loading was weld rupture, while for compression loading it was bolt fracture. The addition of axial load decreased the shear strength, and this effect was more pronounced for tensile loading and deeper connections.

Salem (2016) conducted experimental and finite element analysis (FEA) with both semi-rigid and rigid support conditions. It was observed that for a rigid support condition, an increase in compression force caused a rapid decrease in shear strength. On the other hand, for a semi-rigid support, the addition of compression increased the strength. However, it should be noted that testing was done for only one level of compression load, so no definitive conclusions can be drawn about the actual behavior under combined loading.

Nasrabadi (2018) conducted experimental and FEA on various cases of extended shear tabs, including the unstiffened configuration. The results revealed that the application of axial compression either decreased or increased the ultimate strength of the connections, depending on the intensity of the axial force and on the mode of failure experienced under the application of a pure shear load. Conversely, the application of axial tension decreased the strength in all cases. For a connection whose failure mode was buckling under shear load alone, its strength decreased. However, for a connection with net section rupture as the failure mode, its strength increased for a level of force up to 37% of the axial yield strength.

AVAILABLE INTERACTION EQUATIONS FOR DESIGN UNDER COMBINED SHEAR AND AXIAL FORCES

There are several interaction equations in the 16th Edition of the AISC *Steel Construction Manual* (2023), hereafter referred to as the AISC *Manual*. The first, AISC *Manual* Equation 10-8, shown as Equation 1, includes only the interaction of shear and flexural yielding. It does not include the case of axial loading. The second, AISC *Manual* Equation 9-1, shown as Equation 2, is included for the interaction of shear, moment, and axial load for the case of in-plane loading only. Design considerations for extended single-plate shear connections subjected to combined shear and axial forces have been incorporated in the newly added Part 12 of the AISC *Manual*, which suggests using Equations 12-2 and 12-3 to check the plate for the interaction of axial force (tension and compression), shear force, and flexure for yielding and lateral torsional buckling. These equations, listed as Equations 3 and 4, are derived from AISC *Specification for Structural Steel Buildings* (AISC, 2022a) Chapter H, in conjunction with AISC *Manual* Equation 10-8. They include the minor-axis flexural term, wherein the required flexural strength is calculated by using the geometric horizontal eccentricity. Additionally, the AISC *Manual* suggests that the weak-axis flexural term need not be included in the strength check whenever a slab is present at the top of the supported beam and there is sufficient restraint against the rotation about its longitudinal axis. The use of these equations can be found in the AISC *Companion to the Steel Construction Manual*, Example IIA-19B (2022b), to check for the interaction of axial, shear, and flexural yielding of the plate, as well as rupture of the plate. It assumes the case where a slab is present at the top of the beam, providing sufficient restraint against minor-axis rotation, and completely ignores the minor-axis flexural term in the equation. Equations 3 and 4 will take the form of Equations 5 and 6 when the weak-axis flexural term is ignored in the equation.

None of the AISC *Manual* equations have included torsional load into the interaction equations applicable to extended shear tabs. Dowswell (2019) proposed an interaction equation for an extended shear tab under combined loading by explicitly including the torsional term, as shown in Equation 7. This equation also uses geometric

eccentricity to calculate the torsional moment. However, no experimental or finite element studies have been performed to validate the effectiveness of these equations in predicting the strength of extended shear tabs subjected to combined shear and axial force.

$$\left(\frac{V_r}{V_c}\right)^2+\left(\frac{M_r}{M_c}\right)^2\le 1.0 \tag{1}$$

$$\frac{M_r}{M_c}+\left(\frac{P_r}{P_c}\right)^2+\left(\frac{V_r}{V_c}\right)^4\le 1.0 \text{ for } \frac{P_r}{P_c}<0.2 \tag{2}$$

$$\left(\frac{P_r}{2P_c}+\frac{M_{rx}}{M_{cx}}\right)^2+\left(\frac{V_r}{V_c}\right)^2\le 1.0 \text{ for } \frac{P_r}{P_c}<0.2 \tag{3}$$

$$\left(\frac{P_r}{2P_c}+\frac{8}{9}\frac{M_{rx}}{M_{cx}}\right)^2+\left(\frac{V_r}{V_c}\right)^2\le 1.0 \text{ for } \frac{P_r}{P_c}\ge 0.2 \tag{4}$$

$$\left[\frac{P_r}{2P_c}+\left(\frac{M_{rx}}{M_{cx}}+\frac{M_{ry}}{M_{cy}}\right)\right]^2+\left(\frac{V_r}{V_c}\right)^2\le 1.0 \text{ for } \frac{P_r}{P_c}<0.2 \tag{5}$$

$$\left[\frac{P_r}{2P_c}+\frac{8}{9}\left(\frac{M_{rx}}{M_{cx}}+\frac{M_{ry}}{M_{cy}}\right)\right]^2+\left(\frac{V_r}{V_c}\right)^2\le 1.0 \text{ for } \frac{P_r}{P_c}\ge 0.2 \tag{6}$$

$$\left(\frac{P_r}{P_c}\right)^k+\left(\frac{T_r}{T_c}\right)^2+\left(\frac{V_r}{V_c}\right)^4+\left[\left(\frac{M_{rx}}{M_{cx}}\right)^{1.7}+\left(\frac{M_{ry}}{M_{cy}}\right)^{1.7}\right]^{0.59}\le 1.0 \tag{7}$$

$$M_{ry}=P_r\left(\frac{t_p+t_w}{2}\right) \tag{8}$$

where

$k = 1$ for compressive load

$= 2$ for tensile load

RESEARCH SIGNIFICANCE

Based on the literature study, it was found that there are only a few research programs that have been conducted to study the behavior of extended shear tabs subjected to combined shear and axial forces. The studies done in the past were mostly qualitative in nature where the specimens were not subjected to a range of axial loads. The available results from past research programs show that axial load will influence the ultimate strength and failure mode of the connection. The AISC 15th Edition *Manual* (2017) did not include the case of axial loading in the design procedure for extended shear tabs. The newly added Part 12 in the AISC 16th Edition *Manual* (2023) now includes Equations 5 and 6 to consider the interaction of shear, axial, and flexural forces. However, no experimental and analytical studies have been performed to validate the use of these equations. This study aims to understand the behavior of extended shear tabs subjected to combined shear and compression forces and validate the use of these interaction equations.

Finite element analyses by Rahman et al. (2007) identified the relevant parameters, such as the coefficient of friction, boundary conditions, element types, and loading steps for finite element modeling of extended shear tabs. The work done by Thomas (2014), Salem (2016), and Nasarbadi (2018) concluded that finite element models can accurately predict the results of the experimental testing done in extended shear tabs subjected to combined loading of shear and compression forces as well. Because experimental testing for the case of combined loading is very difficult and expensive, finite element analysis is a valuable tool to study the behavior of extended shear tabs under combined shear and compression forces.

TEST MATRIX AND FINITE ELEMENT ANALYSIS

Test Matrix

Table 1 shows the test matrix that was developed to study the behavior of the extended shear tabs subjected to combined shear and compression forces. The test matrix was developed based on commonly used practical connection components. The three major variables are column web stiffness, connection configuration, and lateral bracing condition of the beams. For each of the connection configurations, the size of the beams, plate thickness, and depth of the plate were made constant.

Figures 3, 4, and 5 show the three connection configurations contained in the test matrix. The two columns selected for the study were W14×233 and W14×90. They are representative of columns used for heavy loads and light loads, respectively, and also provide a range of support condition flexibility. Each 10-ft-long column was connected to three different beam sizes through three different connection configurations. Each case was analyzed for three different practical beam bracing conditions, for a total of 18 cases. Connections 1 and 4, 2 and 5, and 3 and 6 are identical to each other, with the exception of the column size.

Finite Element Modeling in ABAQUS

Previous work by the authors (Ruffley, 2011; Ganaganur Anantharam, 2022) amply demonstrated the capabilities of the finite element modeling approach employed in this work, as also supported by Rahman et al. (2007), among many. The following provides a detailed summary of the modeling approach employed.

Table 1. Test Matrix				
Column Size	**Beam Size**	**Connection ID**	**Connection Configuration**	**Bracing Condition of the Beam**
W14×90	W14×30 Length = 21 ft	Connection 1	3 rows of 2 bolts (total of 6 bolts), ⅜ in. plate	i. Top flange continuously braced ii. One-point lateral restraint on top flange near the connection end iii. No lateral restraint on top flange
	W18×35 Length = 27 ft	Connection 2	4 rows of 2 bolts (total of 8 bolts), ½ in. plate	i. Top flange continuously braced ii. One-point lateral restraint on top flange near the connection end iii. No lateral restraint on top flange
	W24×76 Length = 36 ft	Connection 3	5 rows of 2 bolts (total of 10 bolts), ⅝ in. plate	i. Top flange continuously braced ii. One-point lateral restraint on top flange near the connection end iii. No lateral restraint on top flange
W14×233	W14×30 Length = 21 ft	Connection 4	3 rows of 2 bolts, (total of 6 bolts) ⅜ in. plate	i. Top flange continuously braced ii. One-point lateral restraint on top flange near the connection end iii. No lateral restraint on top flange
	W18×35 Length = 27 ft	Connection 5	4 rows of 2 bolts (total of 8 bolts), ½ in. plate	i. Top flange continuously braced ii. One-point lateral restraint on top flange near the connection end iii. No lateral restraint on top flange
	W24×76 Length = 36 ft	Connection 6	5 rows of 2 bolts (total of 10 bolts), ⅝ in. plate	i. Top flange continuously braced ii. One-point lateral restraint on top flange near the connection end iii. No lateral restraint on top flange

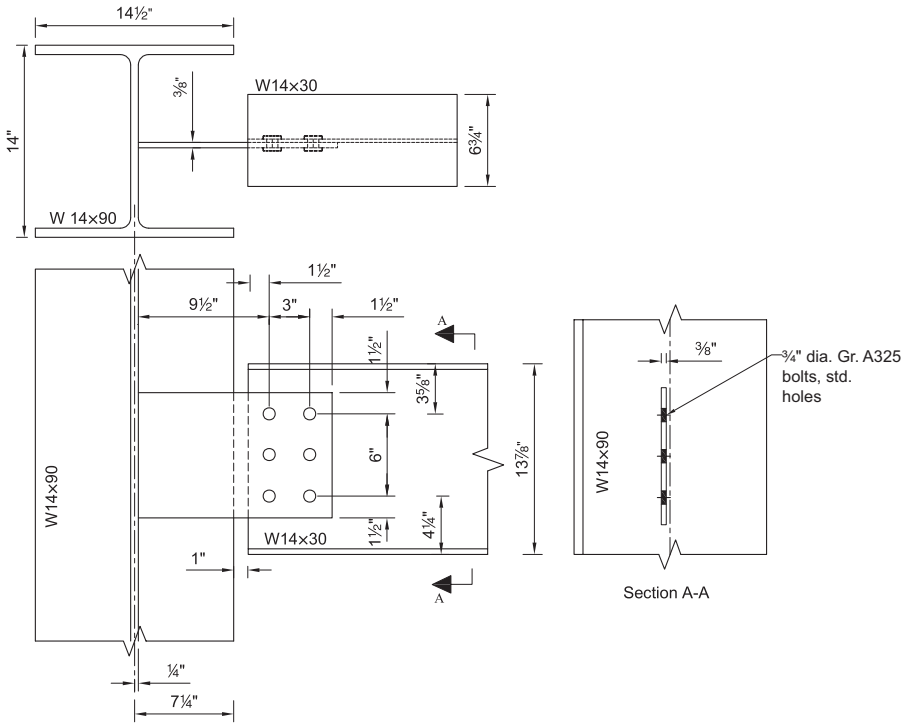

Fig. 3. Connection configuration 1.

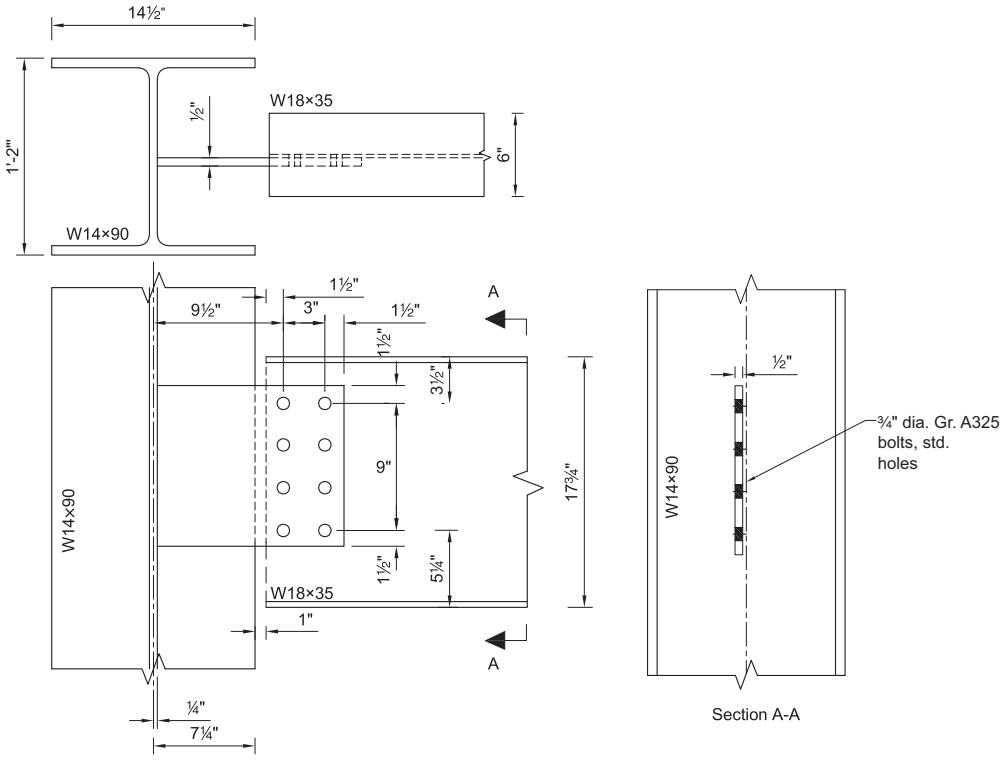

Fig. 4. Connection configuration 2.

Parts, Partitions, Assembly, and Meshing

Parts were created in ABAQUS for each component of a connection using the geometric properties provided in the AISC *Manual* (2017). Partitioning for beams, columns, bolts, and plates was done to achieve a better mesh quality. Beams were modeled only up to half of their length by applying a symmetric restraint at the midspan. To achieve a finer mesh near the connection end and a coarser mesh elsewhere, two separate parts of the beam were created: one with a length equal to twice the depth of the beam, d_b, and other for the remaining length. These parts were then connected using a tie constraint. The same process was followed for the column. The mesh size used in the model is shown in Table 2.

Material Properties

The material model for the beam, column, and plate was taken from the experimental data of past coupon testing done at the University of Cincinnati for an unrelated project, which is shown in Table 3. The tested coupon was ASTM A572/A572M Gr. 50 (2021) steel and was used for both the shear plate and the I-shapes. The measured tensile yield stress and tensile strength were 55.1 ksi and 67.4 ksi, respectively. Similarly, Table 4 shows the material model for bolts that was taken from experimental bolt testing done at the University of Cincinnati. The tested bolts material was ASTM F3125 Gr. A325 (2023) with an ultimate strength of 120 ksi. The measured tensile yield stress and tensile strength were 99.0 ksi and 130 ksi, respectively.

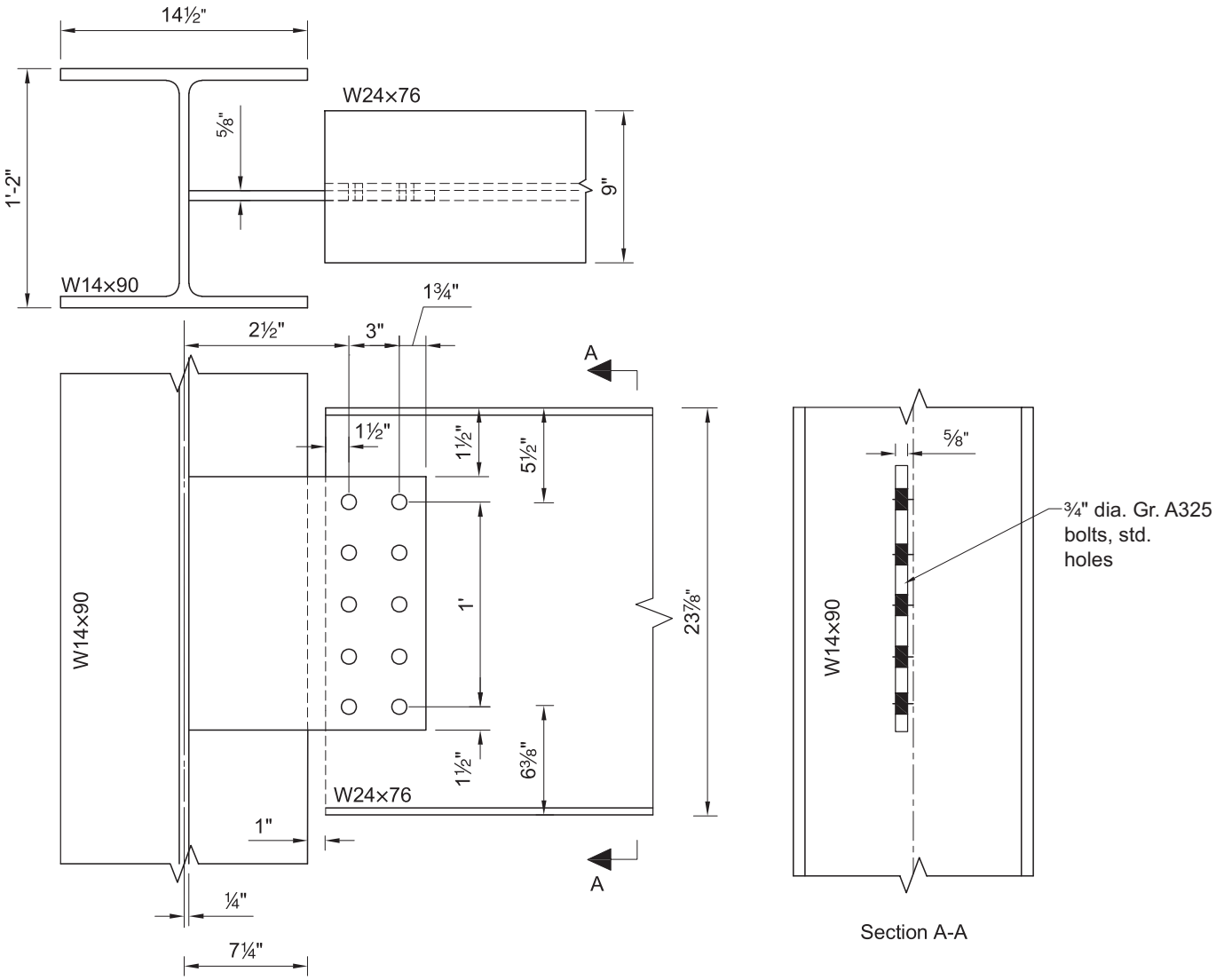

Fig. 5. Connection configuration 3.

Table 2. Mesh Size		
Connection Component	**Partitions**	**Mesh Size, in.**
Beam	$2d_b$ distance	0.2
	Remaining length	0.8
Columns	$3d_b$ distance	0.2
	Remaining length	0.8
Bolts		0.07
Plates		0.15

Table 3. Material Properties for ASTM A572/A572M Gr. 50 and ASTM A992/A992M (2022) Steel				
Engineering Stress, ksi	**Engineering Strain**	**True Stress, ksi**	**True Strain, (in./in.)**	**Plastic Strain (in./in.)**
0	0	0	0	0
55.1	0.00175	55.1	0.00175	0
55.0	0.0305	56.7	0.0300	0.028296
60.5	0.0500	63.5	0.0488	0.047042
65.7	0.100	72.3	0.0953	0.093562
67.0	0.150	77.1	0.140	0.138013
67.4	0.200	80.9	0.182	0.180573
66.5	0.250	83.1	0.223	0.221395
61.7	0.300	80.2	0.262	0.260616
44.3	0.350	59.8	0.300	0.298356
0.0	0.350	0.0	0.300	0.298357

Table 4. Material Properties for ASTM F3125 Gr. A325 Bolts				
Engineering Stress, ksi	**Engineering Strain (in./in.)**	**True Stress, ksi**	**True Strain (in./in.)**	**Plastic Strain (in./in.)**
0	0	0	0	0
99.1	0.00256	99.3	0.00255	0
114.3	0.00704	115.1	0.00701	0.00446
120.7	0.02333	123.6	0.0231	0.0205
128.4	0.04039	133.6	0.0395	0.0370
130.0	0.06315	138.2	0.0612	0.0587
119.1	0.12577	135.1	0.118	0.116
99.2	0.18271	117.3	0.168	0.165
80.3	0.22200	98.2	0.200	0.198

Contact Interaction

Contact interaction among the bolts, plate, and beam web was simulated by creating a contact pair and assigning a interaction property to each contact pair for both normal and tangential behavior. Based on the research of Rahman et al. (2007), the coefficient of friction assigned for tangential behavior was 0.3. "Hard contact" was assigned as the normal behavior.

Based on the study by Ruffley (2011), 3D solid, first-order elements have been used in this work. Reduced integration was used instead of fully integrated first-order elements to avoid the stiff response of the elements in bending, which is known as "shear locking." However, first-order linear elements with reduced integration (C3D8R) are sensitive to hour-glassing; the effect resulting in elements with no stiffness when subjected to bending (Mirzaei, 2014). ABAQUS has hourglass control available to reduce this effect. Taking all of these into consideration, the element type used in the analysis was a 3D solid, linear brick element with reduced integration and hourglass control.

Restraints, Constraint, Analysis Step, and Loading

A reference point was provided at the centroid of the end surface of the beam and column. The nodes of the end surface of the beam and column were coupled to the respective reference point by using a kinematic coupling constraint. The boundary conditions and load were then applied to the reference point. The weld between the plate and the column web was not explicitly modeled. The weld's behavior was simulated by using a tie constraint between the plate end surface (slave surface) and the column web surface (master surface). The displacement at the column ends was restrained in all three directions, and rotation was restrained about the longitudinal axis of the column. The beam free end was provided with a XSYM (U1 = UR2 = UR3 = 0) boundary condition enforcing symmetry in a plane transverse to the axis of the beam.

In addition, to prevent lateral buckling failure of the beams under compressive load, lateral restraints were applied. The W14×30 beam was restrained at two points, the W18×35 at four points, and the W24×76 at three points along the span at a uniform spacing. To achieve a lateral restraint in ABAQUS, the beams were divided into the number of parts equal to the required number of bracings to create a set of nodes. Then, the appropriate boundary condition was applied to the nodes on each division. The number of bracing points was fixed to prevent lateral buckling and to maintain a consistent ratio of L_b/r_y (L_b = unbraced length, and r_y = radius of gyration about the weak axis) for all beams. Similarly, for compression loading, flange buckling was observed in the W14×90 column. Therefore, the flanges of the W14×90 column were restrained in the lateral direction at all nodes along the column flanges to prevent local buckling of the column, which was outside of the scope of this study.

Compressive loading was applied to the beam end, while shear loading was applied as a point load at such a distance from the connection end as to obtain the same shear force and rotation that would be produced by applying a uniformly distributed load over the span. To prevent the lateral torsional buckling failure of the beam, loads were applied 2 ft away from the connection in the beam bracing cases where the top flange is not continuously restrained in the lateral direction.

Loading was applied in two steps—pretensioning and loading—whenever an analysis was run for the case of shear load only. However, when the compression load was included in the analysis, the loading was applied in five steps. The loading protocol for the horizontal loading was taken from research by Mirzaei (2014) where at first the shear load was applied as a displacement-based vertical load up to the service level. After that, the desired compression force (as a percentage of the axial yield strength of the plate) was applied in full as a point load (force-based loading). Finally, the remaining shear load was applied up to failure, keeping the axial load constant.

All analysis steps included geometric nonlinearity. The direct equation solver was used with Full Newton Raphson as the solution technique. The steps in the analysis are further explained in the following:

i. Initial Step

In this step, restraints were applied to the ends of the beam and column. No external load was applied in this step.

ii. Pretensioning Step

In this step, bolts were pretensioned using the temperature method based on the research of Ruffley (2011). Additionally, Ganaganur Anantharam's (2022) research work shows that the temperature method for bolt pretensioning can simulate the most realistic behavior of the pretensioned bolt in all conditions up to failure. In this method, a temperature decrease was applied to the shank of each bolt to achieve the minimum pretension force specified in AISC *Specification* Table J3.1. For ¾-in.-diameter ASTM F3125 Gr. A325 bolts, the minimum pretension force required is 28 kips. The bolts used in the model had threads excluded from the shear plane. The temperature decrease required to achieve this minimum pretension is given by Equation 9. However, this is strictly true only if the materials in the grip are perfectly rigid. So, this equation is only capable of providing an initial estimate of the temperature change required. Following that, a

series of iterations must be performed, decreasing the temperature each time until the required pretension is achieved.

$$\Delta T = \frac{P_b}{E\alpha A_b} \tag{9}$$

where ΔT is the temperature change, P_b is the minimum pretension force, E is the modulus of elasticity of steel = 29,000 ksi, A_b is the area of the bolt shank and α is the coefficient of thermal expansion for steel = $6.6 \times 10^{-6}/°F$. The temperature change required to achieve minimum pretension for a bolt used in the analysis using Equation 10 was found to be 331°F, which was used as an initial estimate of the iterative process. Finally, after several iterations, the temperature change that provides the minimum required pretension was found to be −645°F.

iii. Shear Loading–1

In this step, displacement-based vertical loading was applied to the point of shear loading. Whenever the analysis was performed for the case of combined shear and compression, the shear load was applied only up to the service load level. However, if an analysis was performed for the case of shear load alone, loading was applied up to the failure point of the connection in this step and no further loading step was required.

iv. Notional Load

Geometric imperfections were simulated using the notional load approach. Dowswell (2016) discusses the notional load approach to evaluate the stability of gusset plates. A similar approach has been used in this study. The notional load parameter, ξ, was taken as 0.012. A notional load equal to the required axial strength multiplied by the notional load parameter is applied at the first vertical bolt line in the transverse direction. This load is kept constant for the remainder of the loading step.

v. Compression Loading

In this step, compression load was applied to the reference point attached to the end cross section of the beam as a force-based loading. It was applied as the percentage of the axial yield strength of the plate, P_y. The shear load applied up to the service load level was maintained in this step.

vi. Shear Loading–2

In this step, the remaining shear load was applied to the point of shear loading as a displacement-based loading keeping the compression load constant until failure.

RESULTS AND DISCUSSIONS

In the following section, the results and discussion for the finite element analysis of the connections in the test matrix are presented separately for the three different bracing conditions of the beam.

Beam Bracing Case: Top Flange Continuously Braced

The behavior of the connections was dependent on the column size used when subjected to shear loading. The connection with a W14×90 column showed yielding of the plate at the first vertical bolt line, followed by yielding near the support line, as shown in Figure 6. The figure shows the equivalent plastic strain (PEEQ) in the plate, column web, and beam web, where the light gray color indicates yielding. Significant yielding and rotation of the column web were observed. This caused the point of inflection, initially located between the bolt line and the support line, to further shift toward the support line, which increased the moment at the first vertical bolt line and caused yielding at that location.

All connections with W14×90 column showed similar behavior, except for Connection 3, in which bolt failure occurred before the plate reached net section yielding at the first vertical bolt line. This could be attributed to the use of the actual plate thickness of 0.625 in., which was close to the maximum allowable thickness of 0.63 in. as determined by the AISC (2017) design procedure. The bolt failure occurred at a load of 142 kips, which is 1.21 times the strength obtained by using the design procedure of the AISC 15th Edition *Manual* (2017).

In contrast, the connection with a W14×233 column showed yielding of the gross section near the support line first, followed by yielding of the net section at the first vertical bolt line, as shown in Figure 7. Significant yielding and rotation of the column web were not observed. Large out-of-plane deformation at the bottom of the plate was observed due to the higher negative moment in the plate caused by the stiffer column web.

After analyzing the shear loading case, the connections were subjected to pure compression loading to determine the strength of the plate. To apply a compression load, a displacement was provided at the end of the beam in the negative x-direction. The connections failed due to buckling of the plate.

Once the compressive strength of the plate was determined, the connection was subjected to combined shear and compression forces. The connections were analyzed separately for three cases: shear load plus compression force equal to 25%, 50%, and 75% of the total compressive strength obtained from the previous analysis. The application of compressive forces decreased the shear strength of the plate. The failure mode was lateral buckling of the plate.

The force-displacement plot for shear loading and combined loading cases for Connection 1 is shown in Figure 8. The behavior was further studied by generating an interaction plot, which was normalized against the shear yield strength and axial yield strength of the plate as shown in Figure 9.

The comparison of interaction plots for two different columns is shown in Figures 10 and 11. The figures show that at the lower level of compression force, the rate of decrease in shear strength for the rigid support is greater than that for the flexible support. The reason for the higher effect of the compression force on connections with the W14×233 column is the higher negative moment that develops in the connection caused by the rigidity of the column web. This higher negative moment leads to a higher compression force at the bottom of the plate, which interacts with the applied compression force, ultimately resulting in a buckling failure of the plate. At a higher level of compression force, its effect is seen more for a flexible support. However, in the case of Connection 6, its behavior is similar to that of the connection with the W14×90 column.

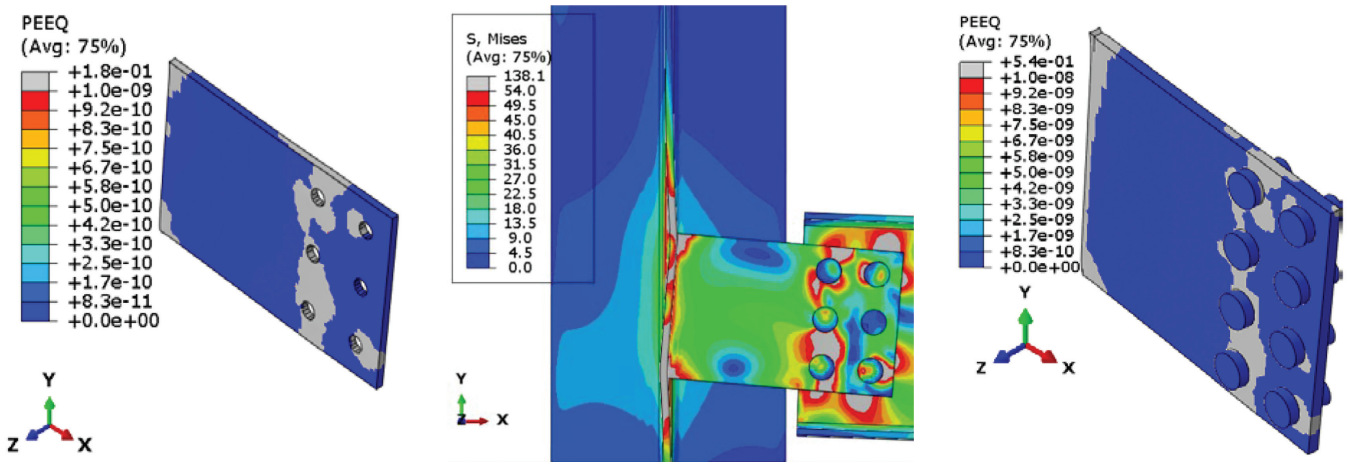

(a) Yielding at net section, Connection 1

(b) Rotation and yielding of column web, Connection 1

(c) Yielding at gross section, Connection 2

Fig. 6. Behavior of connections with W14×90 column.

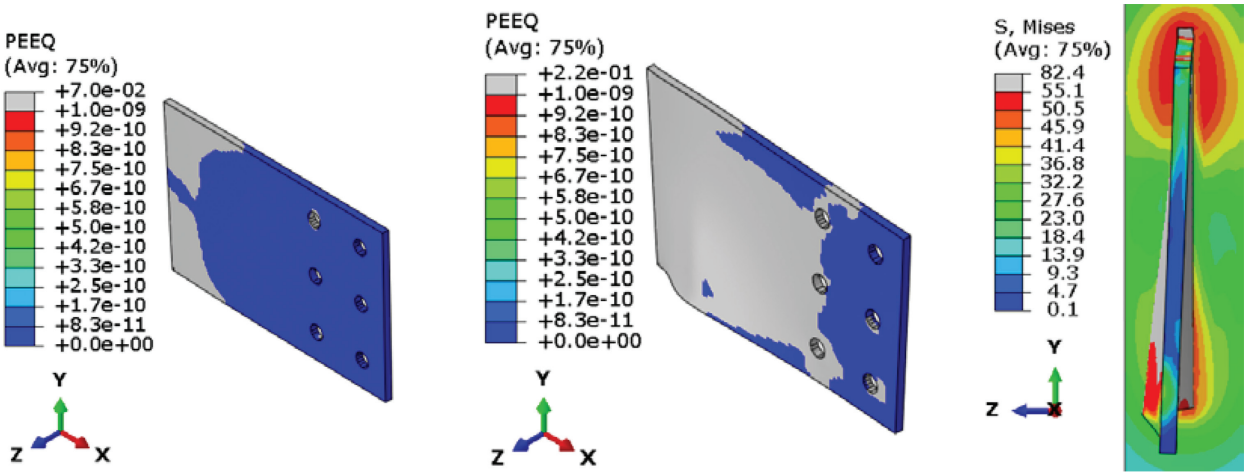

(a) Yielding at the gross section, Connection 4

(b) Yielding at net section, Connection 4

(c) Large out-of-plane deformation at the bottom of the plate, Connection 4

Fig. 7. Behavior of connections with W14×233 column.

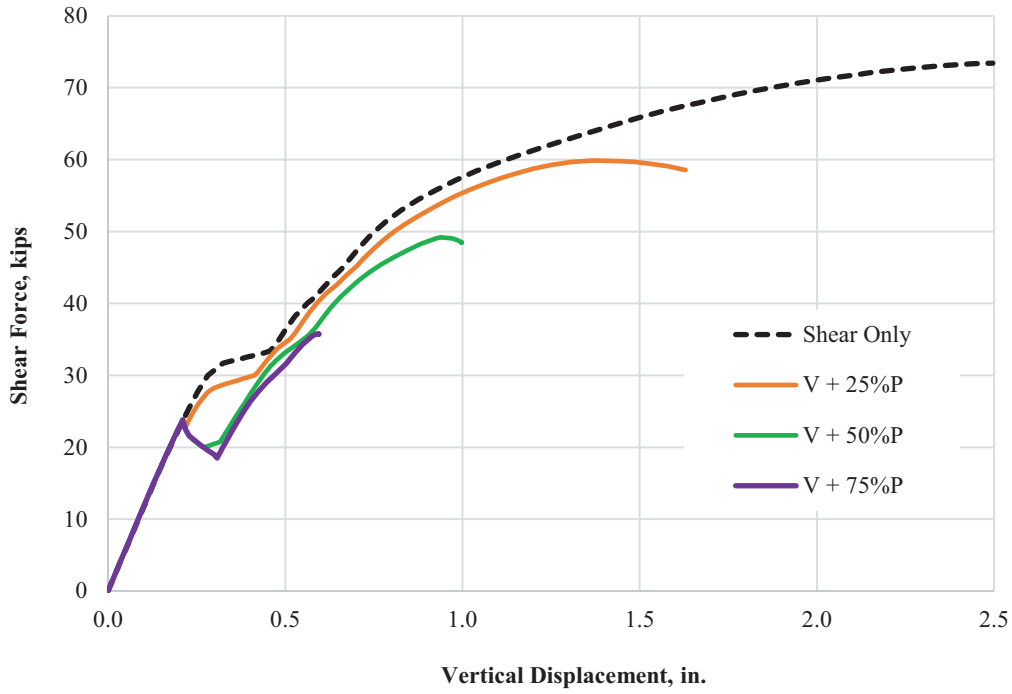

Fig. 8. Force-displacement plot for combined loading for Connection 1.

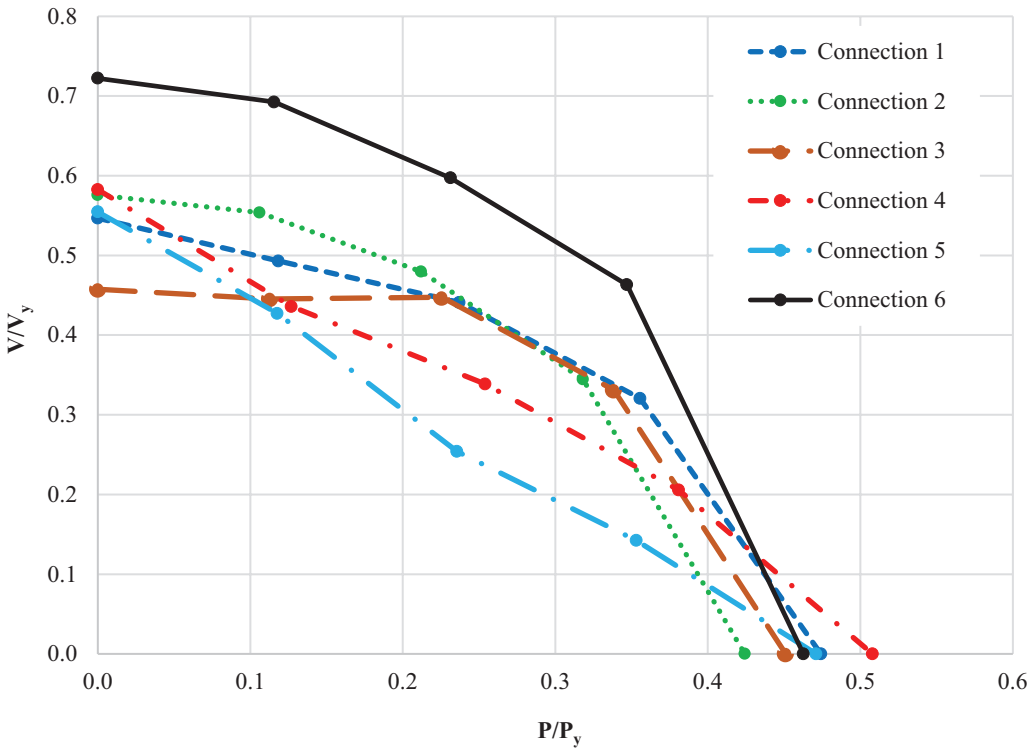

Fig. 9. Normalized shear-compression interaction plot (top flange continuously restrained case).

The comparison of the results from FE analysis with those of the different interaction equations discussed earlier is shown in Table 5. The ratio given in the table is the ratio of the strength obtained from FEA analysis to the results obtained by using the respective interaction equations. The design strength was used in the interaction equation for each term. The value of the resistance factor, ϕ, used for axial, flexural, and torsional strength, was 0.90, while 1.0 was applied for shear yielding strength. The AISC *Manual Companion* Example IIA-19B (2022b) was used to compute the required force and available strength. The flexural strength was determined using AISC *Specification* Section F11, where the limit state of flexural yielding governed for all connection configurations. To compute

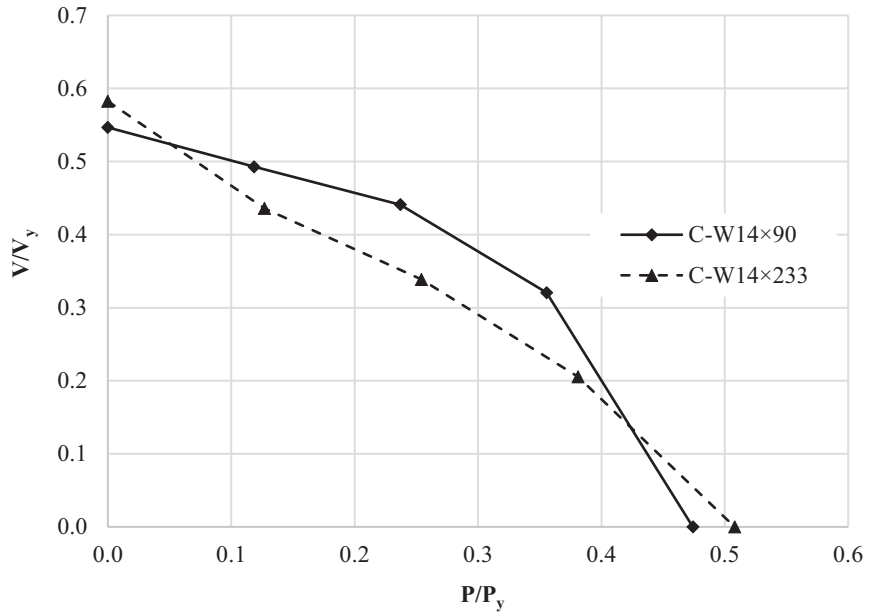

Fig. 10. Comparison of behavior of connection with a six-bolt configuration with W14×90 and W14×233 columns.

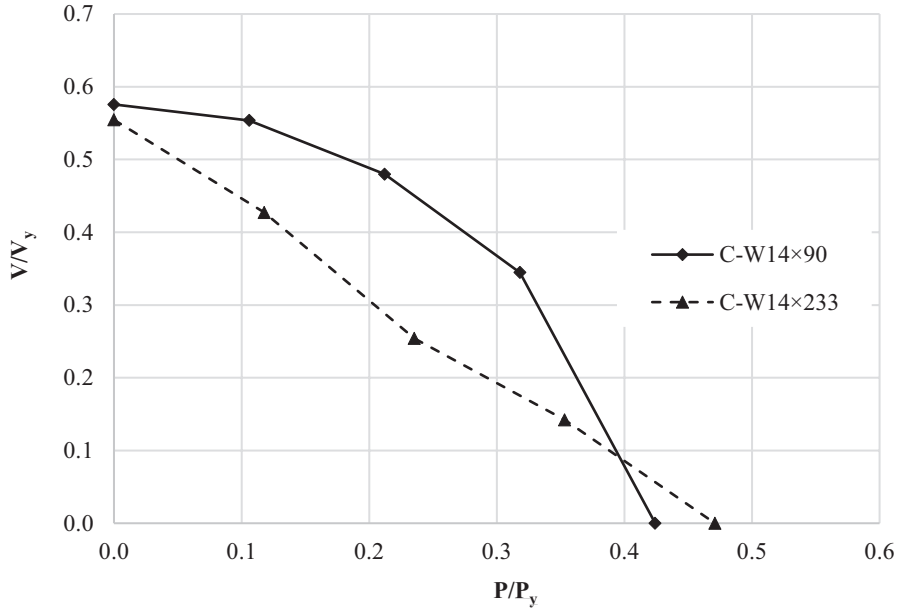

Fig. 11. Comparison of behavior of connection with an eight-bolt configuration with W14×90 and W14×233 columns.

Table 5. Comparison of Results with Interaction Equations for Top Flange Continuously Restrained							
				AISC *Manual* (2023) Eq. 9-1	Dowswell (2019)	AISC *Manual* (2023) Part 12	AISC *Manual* (2023) M_{ry} = 0 Case
	P/P_y	P, kips	V_{FEA}, kips	Ratio	Ratio	Ratio	Ratio
Connection 1	0.00	0.00	55.80	1.43	1.57	1.49	1.49
	0.12	22.04	55.00	1.57	1.87	4.57	1.91
	0.24	44.09	49.20	2.14	6.84	—	3.18
	0.36	66.13	35.78	12.78	—	—	23.20
	0.47	88.17	0.00	1.29	1.93	2.90	1.29
Connection 2	0.00	0.00	114.20	1.27	1.40	1.34	1.34
	0.11	35.06	109.85	1.26	1.53	2.35	1.42
	0.21	70.12	95.18	1.23	2.32	—	1.60
	0.32	105.18	68.36	1.12	—	—	1.65
	0.42	140.24	0.00	0.78	1.64	2.12	0.78
Connection 4	0.00	0.00	65.00	1.72	1.89	1.80	1.74
	0.13	23.62	48.64	1.46	1.76	5.15	1.75
	0.25	47.24	37.79	1.89	—	—	2.80
	0.38	70.85	22.93	—	—	—	—
	0.51	94.47	0.00	1.38	2.06	3.10	1.38
Connection 5	0.00	0.00	110.00	1.26	1.39	1.34	1.34
	0.12	38.93	84.73	1.02	1.30	2.13	1.17
	0.24	77.85	50.38	0.70	—	—	0.94
	0.35	116.78	28.20	0.54	—	—	0.82
	0.47	155.70	0.00	0.87	2.04	2.35	0.87
Connection 6	0.00	0.00	223.00	1.37	1.50	1.45	1.45
	0.12	59.75	214.62	1.35	2.06	2.75	1.52
	0.23	119.50	185.09	1.27	—	—	1.62
	0.35	179.25	143.55	1.18	—	—	1.68
	0.46	239.00	0.00	0.71	2.00	2.27	0.71

lateral-torsional buckling strength, the value of the bending modification factor, C_b was used as 1.84 (Dowswell, 2019). Similarly, the compressive strength of the plate was computed using AISC *Specification* Section J.4 (2016), with the effective length factor, k, set to 1.2. Because all the connection configurations had the ratio of effective length, L_c, to radius of gyration, r, greater than 25, AISC *Specification* Section E3 was applied. The strength was computed using the realistic material properties used in the analysis. It shows that AISC *Manual* Equations 12-2 and 12-3 (Equations 3 and 4) with a case of M_{ry} = 0 and AISC *Manual* Equation 9-1 (Equation 2) can safely predict the strength for a lower level of compression force. However, they can overpredict the strength for a higher level of compression force. Moreover, when the connection involves a larger column web stiffness, increased negative moment in the plate was observed due to the increased rigidity in the connection This resulted in a higher effect of the applied compression force on overall strength of the plate, causing FEA results to be lower than those predicted by the equations.

Since the equations were overpredicting strength for compression loading alone, it became apparent that equations incorporating out-of-plane moments were necessary. The AISC *Manual* interaction Equations 12-2 and 12-3 (Equations 5 and 6) were found to be excessively conservative when the weak-axis flexural term is included in the equation. Dowswell's (2019) equation (Equation 7) was slightly less conservative than the AISC *Manual* Equations 12-2 and 12-3 (Equations 5 and 6), but in some cases of combined loading, the results were still quite conservative.

Beam Bracing Case: Without Lateral Restraint on Top Flange

The failure mode for all connections when subjected to shear loading was twisting of the extended shear tab. The failure load for all connections is given in Table 6 on page 211. The force-displacement plot for shear loading and combined loading cases for Connection 1 is shown in Figure 12. The failure load was taken as the peak load in the force-displacement plot. The deformation in the plate and stress contour for connections 1 and 4 at the peak load is shown in Figure 13.

After analyzing the connection under shear load only, the connections were subsequently subjected to compression load and combined shear and compression forces. Once again, the connections were analyzed separately for three different cases: shear load plus compression force equal to 25%, 50%, and 75% of the total compressive strength obtained from the analysis. The application of compression force resulted in a decrease in the shear strength of the plate, with a greater effect observed at a higher level of compression force. A shear-compression interaction plot was generated, which was normalized against the shear yield strength

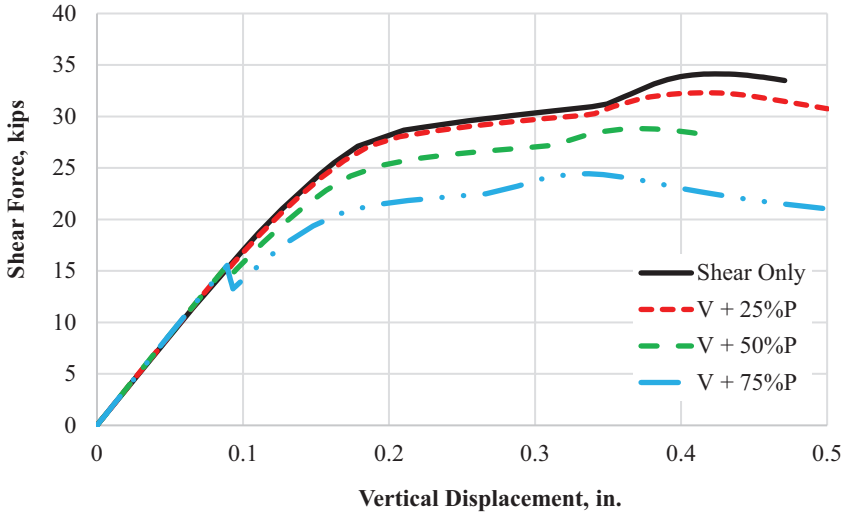

Fig. 12. Force-displacement plot for combined loading for Connection 1.

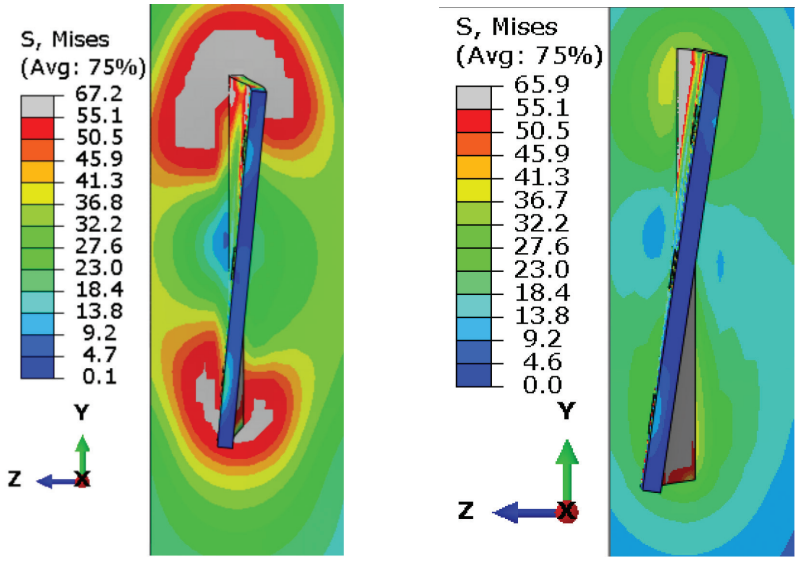

(a) Connection 1 *(b) Connection 4*

Fig. 13. Stress contour plot showing deformation of the plate at peak load.

and axial yield strength of the plate. This plot is presented in Figure 14 for all the connections. The obtained ratio of shear strength to nominal shear yield strength ranged from 0.31 to 0.45, while the obtained ratio of compressive strength to nominal axial yield strength ranged from 0.23 to 0.32.

All three connection configurations were analyzed with the W14×90 column and the W14×233 column. The comparison of interaction plots for two different column sizes is shown in Figures 15, 16, and 17. The figures show that at a lower level of the compression force, the effect of compression force on shear strength is similar for both column sizes. However, at a higher level of compression force, the effect is more pronounced for the flexible column (W14×90).

The comparison of results from the FE analysis with different interaction equations discussed earlier is presented in Table 6. The table shows that the equations that do not include the out-of-plane moment (Equations 2, 3, and 4) consistently overpredict the strength, while Dowswell's (2019) equation (Equation 7) can predict the strength with good accuracy. However, there are some cases where the ratio of observed strength-to-predicted strength is less than 1 by a few percentage points.

Beam Bracing Case: Single Point Restraint Near the Connection

Adding a single point lateral restraint near the connection end prevented the early failure of the connection due to twisting of the plate. The behavior under shear loading was similar to the case of beam bracing, where the top flange was continuously restrained in the lateral direction. The force-displacement plot for shear loading and combined loading cases for Connection 1 is shown in Figure 18. Similarly, Connection 3 failed due to shear failure of the bolt, just like in the beam bracing case with continuous restraint of the top flange.

The application of a compression force results in a decrease in the shear strength of the plate, with the extent of the effect depending on the column size used. A shear-compression interaction plot, normalized against the shear yield strength and axial yield strength of the plate, was generated. This plot is presented in Figure 19 for all connections. The obtained ratio of shear strength to nominal shear yield strength ranged from 0.44 to 0.65, while the obtained ratio of compressive strength to nominal axial yield strength ranged from 0.32 to 0.43.

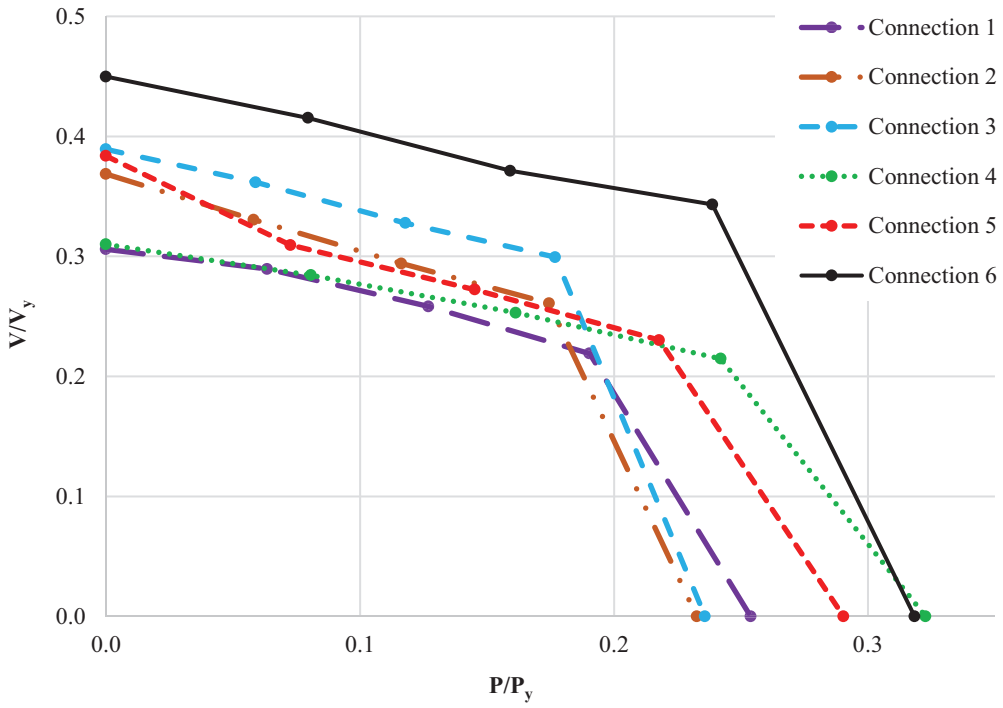

Fig. 14. Normalized shear-compression interaction plot (beam bracing case: without lateral restraint on top flange).

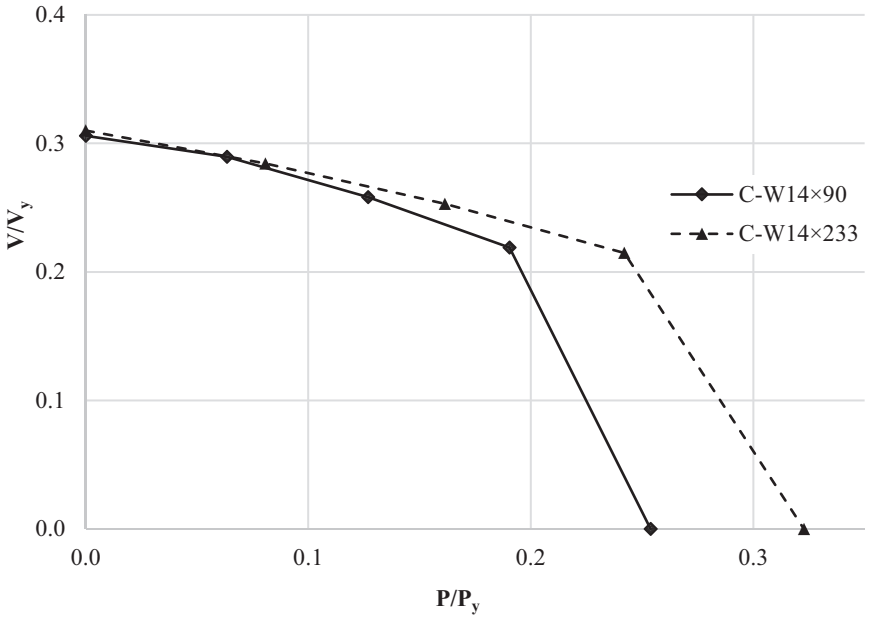

Fig. 15. Comparison of behavior of connection with a six-bolt configuration with W14×90 and W14×233 columns.

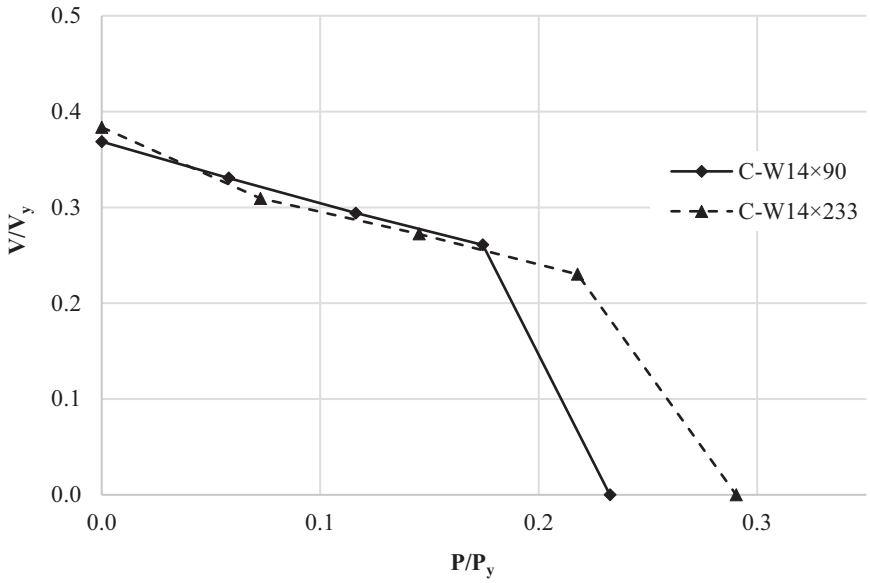

Fig. 16. Comparison of behavior of connection with an eight-bolt configuration with W14×90 and W14×233 columns.

The comparison of interaction plots for two different column sizes is shown in Figures 20 and 21. It was found that the effect of the column size on the behavior of the extended shear tabs under combined loading of shear and compression in this beam bracing case is similar to the beam bracing case where the top flange is continuously braced in the lateral direction. The results show that, at lower levels of compression force, the rate of decrease in shear strength is greater for a rigid support compared to a flexible support. However, at higher levels of compression force, the effect of the compression force was more evident for a flexible support.

The comparison of results from the FE analyses with different interaction equations discussed earlier is shown in Table 7. The observations for a single point restraint in the top flange near the connection end are similar to the case of continuous restraint.

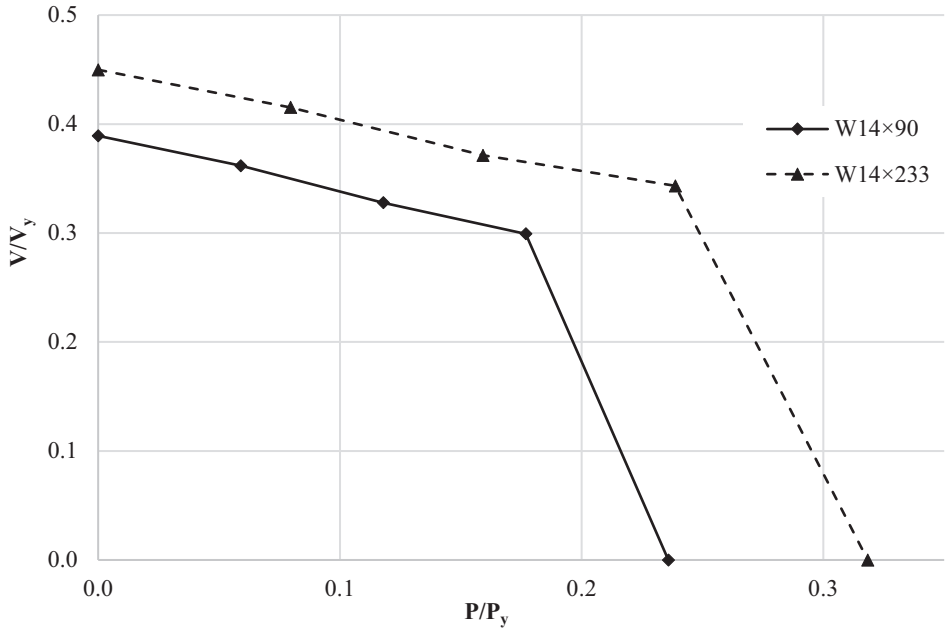

Fig. 17. Comparison of behavior of connection with a 10-bolt configuration with W14×90 and W14×233 columns.

Table 6. Comparison of Results with Interaction Equations for No Restraint on Top Flange							
				AISC *Manual* (2023) Eq. 9-1	Dowswell (2019)	AISC *Manual* (2023) Part 12	AISC *Manual* (2023) $M_{ry} = 0$ Case
	P/P_y	P, kips	V_{FEA}	Ratio	Ratio	Ratio	Ratio
Connection 1	0.00	0.0	34.1	0.87	1.07	0.91	0.91
	0.06	11.8	32.3	0.85	1.10	1.26	0.94
	0.13	23.6	28.8	0.83	1.29	2.93	1.04
	0.19	35.4	24.4	0.85	10.81	—	1.18
	0.25	35.6	47.2	0.69	1.33	1.55	0.69
Connection 2	0.00	0.0	73.1	0.81	1.01	0.86	0.86
	0.06	19.2	65.6	0.74	0.96	1.02	0.81
	0.12	38.5	58.3	0.68	0.98	1.39	0.78
	0.17	57.7	51.8	0.63	1.20	3.89	0.79
	0.23	76.3	76.9	0.43	1.01	1.16	0.43
Connection 3	0.00	0.0	120.6	0.72	0.94	0.76	0.76
	0.06	30.5	112.1	0.67	0.92	0.93	0.74
	0.12	60.9	101.6	0.62	0.96	1.29	0.70
	0.18	91.4	92.8	0.59	1.23	3.47	0.71
	0.24	119.4	121.8	0.36	1.02	1.16	0.36
Connection 4	0.00	0.0	34.6	0.92	1.11	0.96	0.96
	0.08	15.0	31.7	0.88	1.11	1.51	1.00
	0.16	30.0	28.2	0.92	1.31	47.86	1.22
	0.24	45.1	24.0	1.11	5.79	—	1.67
	0.25	45.7	60.1	0.88	1.31	1.98	0.88
Connection 5	0.00	0.0	76.1	0.87	1.08	0.92	0.92
	0.07	24.0	61.4	0.72	0.94	1.07	0.79
	0.15	48.0	54.0	0.66	1.05	2.00	0.79
	0.22	72.0	45.7	0.62	2.36	—	0.80
	0.29	76.3	96.0	0.53	1.26	1.45	0.53
Connection 6	0.00	0.0	139.4	0.86	1.11	0.91	0.91
	0.08	41.1	128.7	0.80	1.53	1.25	0.89
	0.16	82.2	115.1	0.74	1.87	2.74	0.88
	0.24	123.3	106.4	0.74	4.48	—	0.95
	0.32	119.4	164.5	0.73	1.38	1.56	0.49

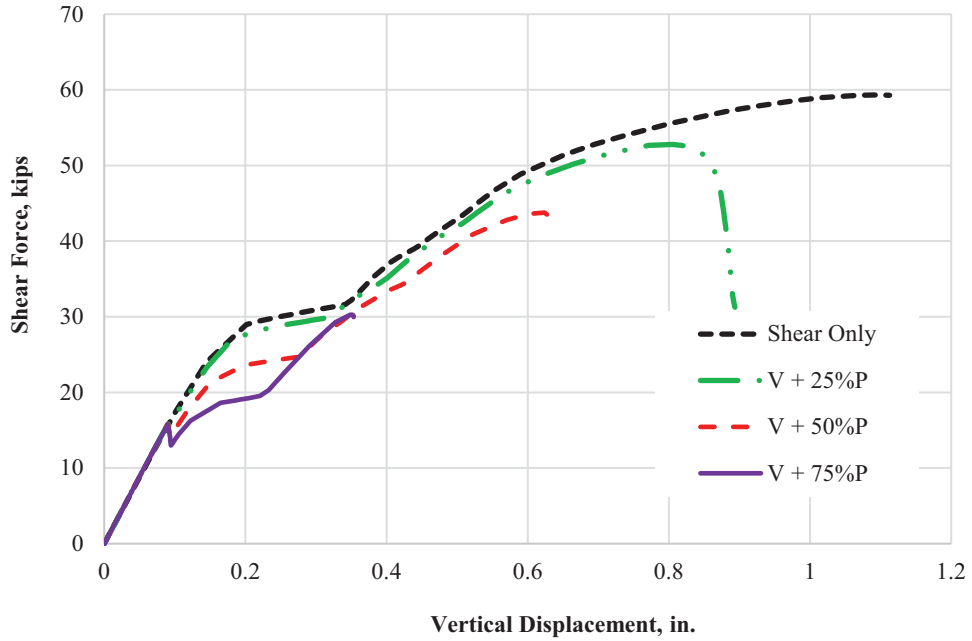

Fig. 18. Force-displacement plot for combined loading for Connection 1.

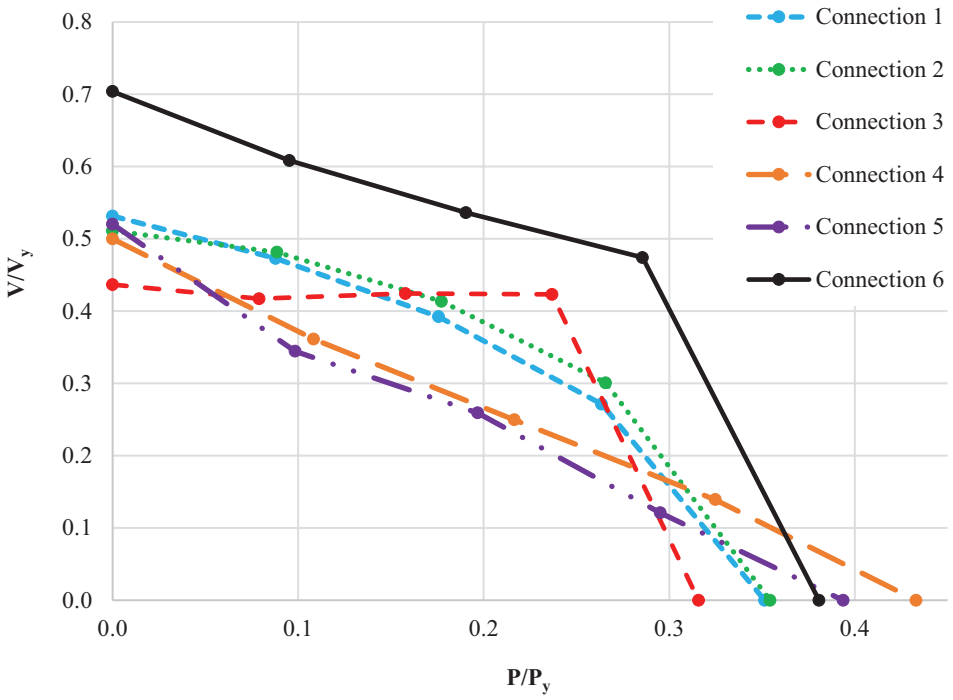

Fig. 19. Normalized shear-compression interaction plot (beam bracing case: single point restraint in top flange near the connection).

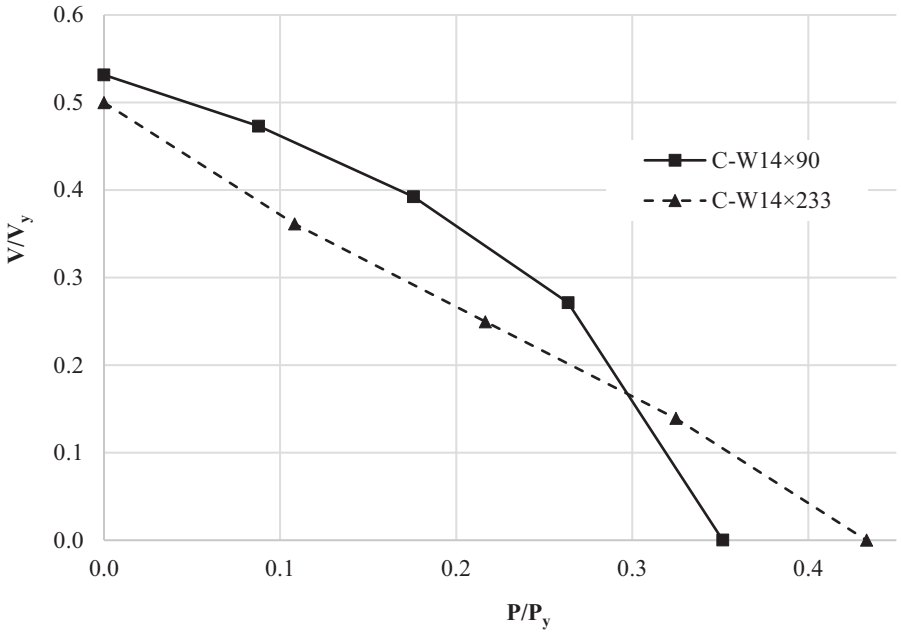

Fig. 20. Comparison of behavior of connection with a six-bolt configuration with W14×90 and W14×233 columns.

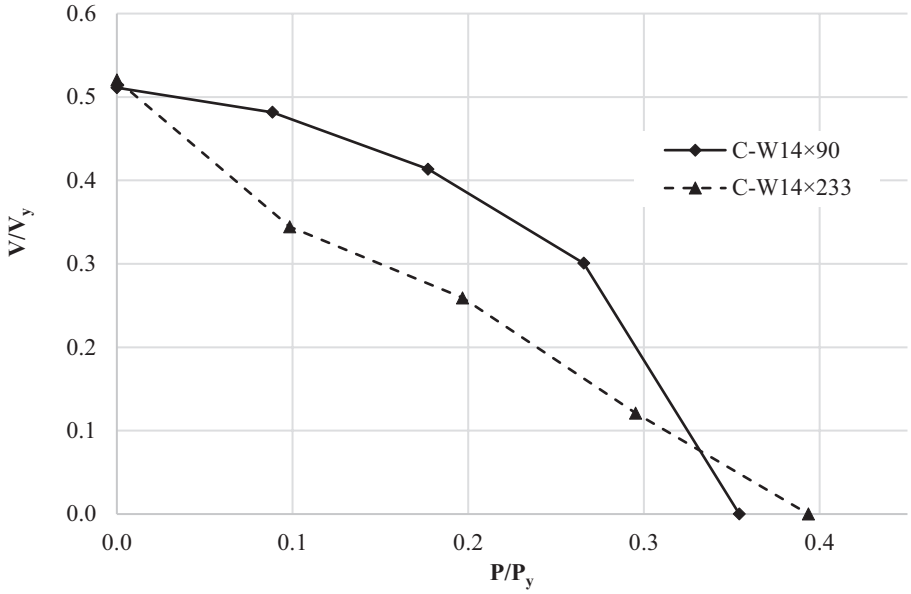

Fig. 21. Comparison of behavior of connection with an eight-bolt configuration with W14×90 and W14×233 columns.

Table 7. Comparison of Results with Interaction Equations for Single Point Restraint on Top Flange Near the Connection							
	P/P_y	P, kips	V_{FEA}	AISC *Manual* (2023) Eq. 9-1	Dowswell (2019)	AISC *Manual* (2023) Part 12	AISC *Manual* (2023) $M_{ry} = 0$ Case
				Ratio	Ratio	Ratio	Ratio
Connection 1	0.00	0.00	59.3	1.52	1.85	1.59	1.59
	0.24	16.33	52.8	1.43	1.93	2.65	1.65
	0.48	32.67	43.8	1.44	4.08	—	1.95
	0.72	49.00	30.3	1.57	—	—	2.44
	0.52	65.33	0.0	0.95	1.84	2.15	0.95
Connection 2	0.00	0.00	101.4	1.13	1.41	1.19	1.19
	0.09	29.28	95.5	1.09	1.48	1.79	1.21
	0.18	58.57	82.0	1.01	1.94	6.87	1.25
	0.27	87.85	59.6	0.85	—	—	1.18
	0.35	117.13	0.0	0.65	1.54	1.77	0.65
Connection 4	0.00	0.00	55.8	1.48	1.62	1.55	1.55
	0.11	20.13	40.3	1.17	1.37	2.84	1.40
	0.22	40.26	27.8	1.12	2.04	—	1.62
	0.32	60.39	15.5	1.83	—	—	3.09
	0.25	80.53	0.0	1.18	1.76	2.65	1.18
Connection 5	0.00	0.00	103.2	1.19	1.47	1.25	1.25
	0.18	32.54	68.3	0.81	1.11	1.43	0.91
	0.36	65.07	51.4	0.67	1.58	30.51	0.85
	0.54	97.61	24.0	0.38	1.20	—	0.55
	0.42	130.14	0.0	0.72	1.70	1.97	0.72
Connection 6	0.00	0.00	218.1	1.34	1.73	1.42	1.42
	0.15	49.17	188.6	1.18	2.33	2.05	1.31
	0.29	98.33	166.2	1.10	3.55	12.52	1.34
	0.44	147.50	147.0	1.08	—	—	1.46
	0.35	196.67	0.0	0.88	1.65	1.87	0.58

Note: Connection 3 results are not reported due to the predicted failure by bolt fracture.

CONCLUSIONS

The major goal of this research was to investigate the behavior of extended shear tab connections when subjected to combined loading of shear and compression forces and to validate the use of available interaction equations. To achieve this goal, 18 finite element models of extended shear tabs with different practical connection configurations were developed and analyzed in ABAQUS for the case of combined loading. The effect of a compression force on the shear strength was studied by analyzing the force-displacement plot, stress contour, deformed shape, and generated shear-compression interaction plot. The results from the analysis were compared with the available interaction equations in the AISC *Manual*, AISC *Specification*, and literature. Based on the research, the following conclusions can be derived:

1. **Effect of the bracing condition of the beam:** The beam bracing condition affects the shear strength and failure mode of the extended shear tabs, be it for shear loading alone or for the combined loading of shear and compression force. The shear strength when no form of bracing is provided in the beam top flange is significantly lower, and connections fail by twisting of the plate. The addition of a single point restraint near the

connection prevents the early twisting failure of the shear tab, and thus significantly improves the shear strength. When the top flange of the beam is continuously braced, the failure mode observed was yielding of the cross section in all cases but one, which failed by bolt fracture.

Use of the interaction equations: Because the shear strength and failure mode of the extended shear tabs depend on the beam bracing condition, different interaction equations are found to be effective for different bracing conditions of the beam. When the top flange of the beam is continuously restrained, equations that do not include the out-of-plane moment terms (AISC *Manual* Equation 9-1, Equations 12-2 and 12-3 with case $M_{ry} = 0$) shown as Equations 2, 3, and 4 herein, can safely predict the strength for a lower level of compression force. However, it can overpredict the strength for a higher level of compression force. Moreover, when the connection involves a column with larger web stiffness, an increased negative moment was observed that resulted in a higher effect of the applied compression force on the shear strength of the plate, causing FEA results to be lower than those predicted by the equations. Since the equation was overpredicting results for compression loading alone, it became apparent that equations incorporating out-of-plane moments were necessary. The equations provided in AISC *Manual* Part 12 that include the weak-axis flexural term (Equations 5 and 6) were found to be overly conservative for this case. Dowswell's (2019) equation (Equation 7) was less conservative than those equations, but in some cases of combined loading, the results were still overly conservative.

When no bracing is provided in the beam top flange, equations that do not include the out-of-plane moments overpredict the strength. In these situations, Dowswell's (2019) equation (Equation 7) can predict the strength with good accuracy.

The conclusions for single point restraint in the top flange near the connection end are similar to those for the continuously restrained case.

2. **Effect of the support condition:** For a top flange that is continuously braced or is braced at a single point near the connection, the effect of a compression force on the shear strength is more significant in the case of a rigid support at a lower level of compression force. As the level of compression force becomes higher, its effect will be higher for a flexible support.

   For a beam unbraced on the top flange, the support condition does not have an influence on the effect of compression force on shear strength for lower levels of compression force. However, for higher levels of compression force, the effect is more evident for flexible columns.

Therefore, while designing, it would be more reliable to use the equation proposed by Dowswell (2019) (Equation 7) to compute the strength safely. Because the results from this equation are much more conservative for cases where continuous or single-point restraint is provided in the top flange, the required weak-axis moment in the equation for these two cases can be decreased to a certain percentage of the value that would have been obtained by using a geometric eccentricity. In this case, decreasing the weak-axis eccentricity to 60% of the geometric eccentricity still yielded an actual-to-predicted strength ratio greater than 1.

SYMBOLS

C_b Bending modification factor

M_c Available plastic moment strength of the plate (kip-in.)

M_{cx} Available strong-axis plastic moment strength of the plate (kip-in.)

M_{cy} Available weak-axis plastic moment strength of the plate (kip-in.)

$M_r = M_u$ Required (ultimate) moment strength of the plate (kip-in.)

$M_{rx} = V_u a$ Required strong-axis moment strength of the plate (kip-in.)

$M_{ry} = P_r\left(\frac{t_p + t_w}{2}\right)$ Required weak-axis moment strength of the plate (kip-in.)

P_c Available axial strength of the plate (kips)

P_r Required axial strength of the plate (kips)

T_c Available torsional strength (kip-in.)

T_r Required torsional strength $= V_r\left(\frac{t_p + t_w}{2}\right)$ (kip-in.)

$V_c = \phi_v V_n$ Available shear yielding strength of the plate (kips)

$V_r = V_u$ Required (ultimate) shear strength (kips)

a Distance from the face of the support to the first vertical line of bolts, in.

d_b Depth of beam, in.

l_{ev} Vertical edge distance, in.

l_{eh} Horizontal edge distance, in.

t_p Thickness of the plate, in.

t_w Thickness of the beam web (in.)

REFERENCES

ABAQUS (2022), *ABAQUS/CAE User's* Guide, Dassault Systemes Simulia Corporation, Waltham, Mass.

AISC (2016), *Specification for Structural Steel Buildings,* ANSI/AISC 360-16*,* American Institute of Steel Construction, Chicago, Ill.

AISC (2017), *Steel Construction Manual,* 15th Ed., American Institute of Steel Construction, Chicago, Ill.

AISC (2022a), *Specification for Structural Steel Buildings,* ANSI/AISC 360-22*,* American Institute of Steel Construction, Chicago, Ill.

AISC (2022b), *Companion to the AISC Steel Construction Manual—Volume 1: Design Examples,* American Institute of Steel Construction, Chicago, Ill.

AISC (2023), *Steel Construction Manual,* 16th Ed., American Institute of Steel Construction, Chicago, Ill.

Asl, M.H., Farivar, B., and Momenzadeh, S. (2019), "Investigation of the Rigidity of Welded Shear Tab Connections," *Engineering Structures*, Vol. 179, pp. 353–366.

ASTM (2021), *Standard Specification for High-Strength Low-Alloy Columbium-Vanadium Structural Steel*, ASTM A572/572M-21e1, ASTM International, West Conshohocken, Pa.

ASTM (2022), *Standard Specification for Structural Steel Shapes*, ASTM A992/A992M, ASTM International, West Conshohocken, Pa.

ASTM (2023), *Standard Specification for High Strength Structural Bolts and Assemblies, Steel and Alloy Steel, Heat Treated, In. Dimensions 120 ksi and 150 ksi Minimum Tensile Strength, and Metric Dimensions 830 MPa and 1040 MPa Minimum Tensile Strength*, ASTM F3125/F3125M, ASTM International, West Conshohocken, Pa.

Dowswell, B. (2016), "A Notional Load Yield Line Model for Gusset Plate Stability," *Proceedings of the AISC North American Steel Construction Conference*, April 13–15, Orlando, Fla.

Dowswell, B. (2019), "Torsion of Rectangular Connection Elements," *Engineering Journal*, AISC, Vol. 56, No. 2, pp. 63–87.

Ganaganur Anantharam, V.A. (2022), "Finite Element Analysis of Stabilizer Plates in Single Plate Shear Connection Using ABAQUS," Master's Thesis, University of Cincinnati, Cincinnati, Ohio.

Mirzaei, A. (2014), "Steel Shear Tab Connections Subjected to Combined Shear and Axial Forces," PhD Dissertation, McGill University, Montreal, Quebec, Canada.

Muir, L.S. and Hewitt, C.M. (2009), "Design of Unstiffened Extended Single-Plate Shear Connections," *Engineering Journal*, AISC, Vol. 46, No. 2, pp. 67–79.

Nasrabadi, M.M. (2018), *Behaviour of Extended Shear Tab Connections under Combined Axial and Shear Forces,* PhD Thesis, McGill University, Montreal, Quebec.

Rahman, A., Mahamid, M., Amro, A., and Ghorbanpoor, A. (2007), "The Analyses of Extended Shear Tab Steel Connections Part I: The Unstiffened Connections," *Engineering Journal*, AISC, Vol. 44, No. 2, pp. 117–132.

Ruffley, D.J. (2011), "A Finite Element Approach for Modeling Bolted Top-and-Seat Angle Components and Moment Connections," Master's Thesis, University of Cincinnati, Cincinnati, Ohio.

Salem, P. (2016), "Unified Design Criteria for Steel Cantilever Plate Connection Elements," PhD Thesis, University of Alberta, Edmonton, Alberta, Canada.

Thomas, K. (2014), "Design and Behaviour of Extended Shear Tabs under Combined Loads," Master's Thesis, University of Alberta, Edmonton, Alberta, Canada.